

How Shift Equivariance Impacts Metric Learning for Instance Segmentation

Josef Lorenz Rumberger^{*1,2}[0000-0002-7225-7011],
 Xiaoyan Yu^{*1,3}[0000-0001-8196-663X],
 Peter Hirsch^{*1,3}[0000-0002-2353-5310],
 Melanie Dohmen^{*1,2,3}[0000-0002-4447-0579],
 Vanessa Emanuela Guarino^{*1,3}[0000-0003-1625-4323],
 Ashkan Mokarian^{1,3}[0000-0001-9166-1039],
 Lisa Mais^{1,3}[0000-0002-9281-2668],
 Jan Funke⁴[0000-0003-4388-7783], and
 Dagmar Kainmueller^{1,3}[0000-0002-9830-2415]

¹ Max Delbrueck Center for Molecular Medicine, Berlin, Germany

² Charité University Medicine, Berlin, Germany

³ Berlin Institute of Health, Berlin, Germany

⁴ HHMI Janelia Research Campus, Ashburn, VA, USA
 {firstnames.lastname}@mdc-berlin.de

Abstract. Metric learning has received conflicting assessments concerning its suitability for solving instance segmentation tasks. It has been dismissed as theoretically flawed due to the shift equivariance of the employed CNNs and their respective inability to distinguish same-looking objects. Yet it has been shown to yield state of the art results for a variety of tasks, and practical issues have mainly been reported in the context of tile-and-stitch approaches, where discontinuities at tile boundaries have been observed. To date, neither of the reported issues have undergone thorough formal analysis. In our work, we contribute a comprehensive formal analysis of the shift equivariance properties of encoder-decoder-style CNNs, which yields a clear picture of what can and cannot be achieved with metric learning in the face of same-looking objects. In particular, we prove that a standard encoder-decoder network that takes d -dimensional images as input, with l pooling layers and pooling factor f , has the capacity to distinguish at most f^{dl} same-looking objects, and we show that this upper limit can be reached. Furthermore, we show that to avoid discontinuities in a tile-and-stitch approach, assuming standard batch size 1, it is necessary to employ valid convolutions in combination with a training output window size strictly greater than f^l , while at test-time it is necessary to crop tiles to size $n \cdot f^l$ before stitching, with $n \geq 1$. We complement these theoretical findings by discussing a number of insightful special cases for which we show empirical results on synthetic data.

Code: https://github.com/Kainmueller-Lab/shift-equivariance_unet

Keywords: Metric Learning · Instance Segmentation · Shift Equivariance

* equal contribution

1 Introduction

Metric learning is a popular and often state-of-the-art proposal-free technique for instance segmentation in the biomedical domain [4,6,9,11,12,15,20]. In discord with its empirical success, numerous works from the computer vision community have noted a theoretical deficiency of metric learning for instance segmentation, namely that same-looking objects cannot be distinguished by means of shift equivariant CNNs [13,15]. Attempts at tackling this apparent deficiency include leveraging pixel coordinates or encodings of said as additional inputs or features [9,14,15,22], or limiting the problem to distinguishing neighboring objects [4,10].

However, while related work has discussed shift equivariance properties of individual CNN layers like pooling [2,21,23] and upsampling [16], what is lacking to date is a comprehensive formal analysis of the shift equivariance properties of the encoder-decoder style CNNs typically employed for metric-learning-based instance segmentation, as well as an assessment of respective implications concerning the capacity of said CNNs to distinguish same-looking objects. In this paper, we prove that an encoder-decoder-style CNN with l pooling layers and pooling factor f is periodic- f^l shift equivariant, and in consequence has the capacity to distinguish at most $f^{d \cdot l}$ instances of identical appearance in d -dimensional input images.

Concerning practical issues, biomedical applications often deal with large 3d input images and thus apply CNNs for instance segmentation in a tile-and-stitch manner to cope with GPU memory constraints. Here, issues with discontinuities in predictions at output tile boundaries, which lead to false splits of objects, have been reported [11,17]. However, again, a formal analysis of the causes is lacking to date. We show that the potential for discontinuities to arise is intricately tied to the shift equivariance properties of the employed CNNs. Our theoretical analysis entails simple rules for designing CNNs that are necessary to avoid discontinuities when predictions are obtained in a tile-and-stitch manner.

2 Formal Analysis of Shift Equivariance Properties

We first define the broad family of U-Net-style encoder-decoder CNNs [18] we consider in our work, followed by a definition of periodic- t shift equivariance. Based on these prerequisites we prove periodic- f^l shift equivariance of U-Nets.

We consider CNNs consisting of l downsampling and l upsampling blocks. A downsampling block consists of a number of conv+nonlinearity layers, followed by max-pooling with downsampling factor (i.e. kernel size and stride) f . An upsampling block consists of a number of conv+nonlinearity layers, followed by upsampling by factor f , either via nearest-neighbor interpolation (*fixed upsampling*) or via transposed convolution (*learnt upsampling*). At each downsampling level of the U-Net, skip connections concatenate the output of the downsampling block before pooling to the input of the respective upsampling block after upsampling, except for the bottom level (also called *bottleneck*). In the following, we refer to any architecture of the above family as a *U-Net*, and to a U-Net with specific weights as a *U-Net instance*. A U-Net has the *capacity* to have some property iff there exists an instance of that U-Net with said property.

If not noted otherwise, we assume that a U-Net outputs all predictions for an image in one go. Sliding-window / tile-and-stitch mode will be discussed in Section 2.1. Furthermore, if not noted otherwise, we assume valid convolutions in all conv layers. Non-valid padding will be discussed in Section 2.2.

Formally, a U-Net is a function U that maps a discrete, d -dimensional input image I with resolution $X_1^{in} \times \dots \times X_d^{in}$ and C^{in} channels to an output image with resolution $X_1^{out} \times \dots \times X_d^{out}$ and C^{out} channels:

$$U : \mathbf{R}^{X_1^{in} \times \dots \times X_d^{in} \times C^{in}} \rightarrow \mathbf{R}^{X_1^{out} \times \dots \times X_d^{out} \times C^{out}} \quad (1)$$

$$I \mapsto U(I) = (\mathbf{u}_{\mathbf{x}}(I))_{\mathbf{x} \in X_1^{out} \times \dots \times X_d^{out}},$$

where

$$\mathbf{u}_{\mathbf{x}} : \mathbf{R}^{X_1^{in} \times \dots \times X_d^{in} \times C^{in}} \rightarrow \mathbf{R}^{C^{out}} \quad I \mapsto \mathbf{u}_{\mathbf{x}}(I) = U(I)(\mathbf{x}) \quad (2)$$

denotes the function that yields the output at output location $\mathbf{x} \in X_1^{out} \times \dots \times X_d^{out}$. Concerning functions $\mathbf{u}_{\mathbf{x}}$, two distinct notions of *equality* can be defined:

Definition 1 (Absolute and Relative Equality). Two functions $\mathbf{u}_{\mathbf{x}_1}, \mathbf{u}_{\mathbf{x}_2}$ are **absolute-equal** iff $\forall I : \mathbf{u}_{\mathbf{x}_1}(I) = \mathbf{u}_{\mathbf{x}_2}(I)$, and **absolute-distinct** otherwise. Two functions $\mathbf{u}_{\mathbf{x}_1}, \mathbf{u}_{\mathbf{x}_2}$ are **relative-equal** iff $\forall I : \mathbf{u}_{\mathbf{x}_1}(I) = \mathbf{u}_{\mathbf{x}_2}(T_{\mathbf{x}_2 - \mathbf{x}_1}(I))$, with $T_{\Delta \mathbf{x}}(I(\mathbf{x})) := I(\mathbf{x} - \Delta \mathbf{x})$ denoting an image shift by $\Delta \mathbf{x}$. Otherwise $\mathbf{u}_{\mathbf{x}_1}$ and $\mathbf{u}_{\mathbf{x}_2}$ are **relative-distinct**.

We provide examples for absolute and relative equality of U-Net functions in Appendix A.1. Following [23], we define *periodic-t shift equivariance* as follows:

Definition 2 (Periodic-t Shift Equivariance). A function F that maps an input image I to an output image $F(I)$ is **periodic-t shift equivariant** iff $F(T_{\Delta \mathbf{x}}(I)) = T_{\Delta \mathbf{x}}(F(I))$ $\forall \Delta \mathbf{x} \in \{(z_1 \cdot t, \dots, z_d \cdot t) \mid z_i \in \mathbf{Z}\}$, and t is the smallest number for which this holds.

Lemma 1 (Relative-distinct functions \mathbf{u} of a U-Net.). Every U-Net has the capacity to implement f^{dl} relative-distinct functions \mathbf{u} , but not more.

Proof. Part I: For any U-Net, we construct an instance and an image I with unique outputs $\mathbf{u}_{\mathbf{x} - \Delta \mathbf{x}}(T_{-\Delta \mathbf{x}}(I))$ for all $\Delta \mathbf{x} \in \{0, \dots, f^l - 1\}^d$, proving that every U-Net has the capacity to implement *at least* f^{dl} relative-distinct functions. Part II: We prove that every U-Net is equivariant to image shifts f^l , and hence *no* U-Net has the capacity to implement *more than* f^{dl} relative-distinct functions.

Proof part I: We construct a U-Net instance and an input image I which yields f^{dl} relative-distinct output function values, as described in the following. Fig. 1 shows a sketch of our construction for $d = 1$. First, for any given U-Net, construct an instance U with fixed upsampling (i.e. all upsampling kernel weights set to 1), all convolutions set to identity, and ignore skip connections by setting respective convolution kernel entries to 0. For a d -dimensional input image I , this U-Net instance yields outputs

$$\mathbf{u}_{\mathbf{x}}(I) = \max\{I(\lfloor \mathbf{x}/f^l \rfloor \cdot f^l + \Delta \mathbf{x}) \mid \Delta \mathbf{x} \in \{0, \dots, f^l - 1\}^d\}.$$

Second, construct a single-channel image I such that $I(\mathbf{x})$ is strictly increasing for increasing positions \mathbf{x} w.r.t. an ordering of positions along diagonals first by the sum of

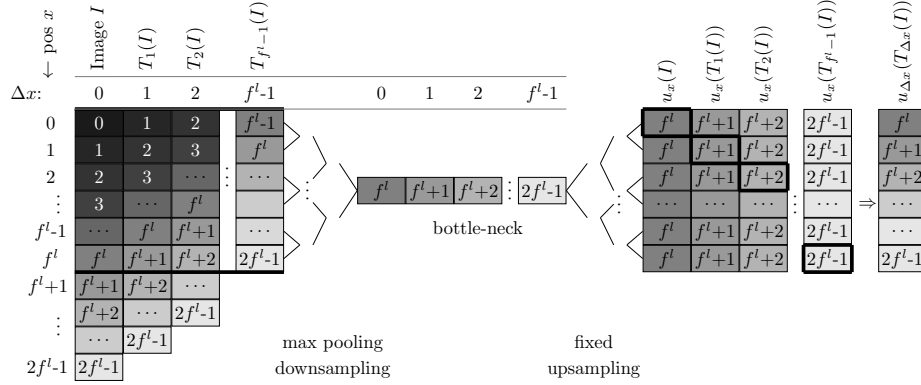


Fig. 1: Illustration of a U-Net instance and a 1-dimensional image I such that the functions $u_{\Delta x}$ are relative-distinct for all Δx with $0 \leq \Delta x < f^l$.

their components and second by their components in increasing order (cf. [3,19]):

$$\mathbf{x}_i > \mathbf{x}_j \iff \begin{cases} \sum_k x_i^{(k)} > \sum_k x_j^{(k)} & \text{if } \sum_k x_i^{(k)} \neq \sum_k x_j^{(k)} \\ x_i^{(k)} > x_j^{(k)} & \text{if } \sum_k x_i^{(k)} = \sum_k x_j^{(k)} \text{ and } x_i^{(l)} = x_j^{(l)} \forall l < k \end{cases} \quad (3)$$

For this image, the maximum intensity in any image pixel block of edge length f^l is found at the maximum position $(f^l - 1, \dots, f^l - 1)^d$. Consequently, as each distinct pixel block of edge length f^l covers a unique maximum position,

$$u_{\mathbf{x}-\Delta \mathbf{x}_i}(T_{-\Delta \mathbf{x}_i}(I)) \neq u_{\mathbf{x}-\Delta \mathbf{x}_j}(T_{-\Delta \mathbf{x}_j}(I)) \forall \mathbf{x} \forall \Delta \mathbf{x}_i \neq \Delta \mathbf{x}_j \in \{0, \dots, f^l - 1\}^d,$$

i.e. the constructed U-Net instance implements f^{dl} relative-distinct functions u .

Proof part II: See Appendix A.2. \square

Corollary 1 (Periodic- f^l Shift Equivariance of the U-Net). *Every U-Net has the capacity to be periodic- f^l shift equivariant.*

Proof. Directly follows from the proof of Lemma 1, which shows in Part I that every U-Net has the capacity to be non-equivariant to any shifts $< f^l$, and in Part II that every U-Net is shift equivariant to shifts f^l . \square

2.1 Tile-and-stitch mode

In practice, to deal with limited GPU memory, a U-Net is commonly trained on fixed-size input image tiles, yielding fixed-size output tiles. At test time, the output for a full input image is then obtained in a tile-and-stitch manner, where it is common to employ the same tile size as during training, yet larger tile sizes are sometimes employed as inference is less memory-demanding than training.

Concerning shift equivariance in a tile-and-stitch approach with output tile size w during inference, we get (1) periodic- f^l shift equivariance within output tiles, and (2) trivially, periodic- w shift equivariance across output tiles. Periodic- f^l shift equivariance across the whole output only holds if w is a multiple of f^l .

2.2 Non-valid padding

The concept of shift equivariance runs counter to the concept of non-valid padding, as non-valid padding does not allow for "clean" input image shifts: Shifting+padding will, in general, change the input image beyond the shift. As a notable consequence, e.g., zero padding renders a CNN with sufficiently large receptive field location-aware [8,1], thus completely breaking shift equivariance. See [8] for an in-depth discussion of zero-padding and other common padding schemes.

3 Impact on Metric Learning for Instance Segmentation

We assess implications of a U-Net's periodic- f^l shift equivariance on the application of instance segmentation via metric learning with discriminative loss [6]. The respective loss function has three terms, a pull-force that pulls pixel embeddings towards their respective instance centroid, a push force that pushes centroids apart, and a penalty on embedding vector lengths. Given predicted embeddings, instances are inferred by mean-shift clustering. For more details, see [6]. First, we assess how many "same-looking" instances a U-Net trained with discriminative loss can distinguish. We call two instances "same-looking" iff the image itself is invariant to shifting by the offset between instance center points. Second, we show the necessity to follow a concise set of simple rules to avoid inconsistencies in a tile-and-stitch approach.

3.1 Distinguishing Same-looking Instances (thus Avoiding False Merges)

Corollary 2. *A U-Net has the capacity to distinguish at most f^{dl} same-looking instances.*

Proof. Lemma 1 entails that a U-Net can assign at most f^{dl} different embeddings to a representative pixel of an object instance (say the "central pixel"), namely when positioned at the f^{dl} different relative locations w.r.t. its max-pooling regions. This holds true iff same-looking instances are located at offsets p with p, f^l co-prime. Whether a U-Net is also able to assign same embeddings to all pixels within any instance, thereby yielding f^{dl} correct segmentations, is up to its capacity and the success of training. \square

Corollary 3. *A U-Net cannot distinguish same-looking instances located at offsets $n \cdot f^l, n \in \mathbf{N}$.*

Proof. Periodic- f^l shift equivariance of the U-Net entails that it necessarily assigns same embeddings to pixels at same relative locations in the objects. \square

Fig. 2 showcases Corollaries 2 and 3 on synthetic images of periodically arranged disks, for which we trained U-Nets with discriminative loss to predict 3-dimensional embeddings. In particular, it shows that the upper bound of separating f^{dl} same-looking instances, as stated in Corollary 2, can be reached.

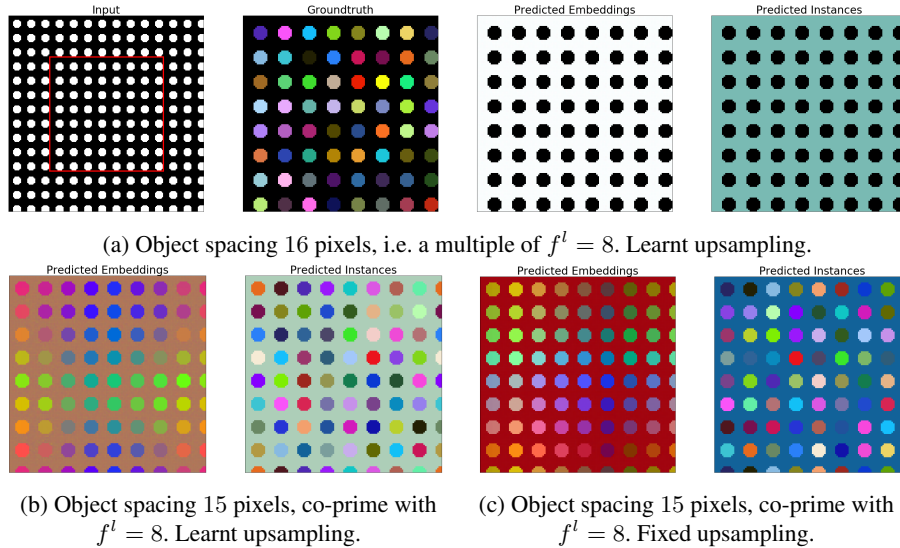


Fig. 2: A U-Net with l pooling layers and pooling factor f cannot distinguish any instances in an f^l -periodic d -dimensional image of same-looking instances (a). However, it can distinguish up to $f^{d \cdot l}$ instances in a p -periodic image of same-looking instances for p, f^l co-prime (b,c). Showcase: $l = 3, f = 2, f^l = 8, f^{dl} = 64$. The red box in the input image (top left) shows the valid output window. Analogous results can be achieved for the same object spacings and $l = 4, f = 2$ (not shown).

3.2 Avoiding False Splits of Instances in a Tile-and-Stitch Approach

In the following, we analyze the impact of output tile size on training with discriminative loss, as well as on inference in a tile-and-stitch manner. To this end, we assess which of the f^{dl} potentially relative-distinct output functions of a U-Net contribute to the loss, and which pairs of functions that predict directly neighboring outputs in a stitched solution may contribute to an instance’s pull force loss term during training.

Training output tile size $< f^l$: In this case, some of the f^{dl} output functions of the U-Net never contribute to the loss, i.e. they are not explicitly trained. In effect, they may yield nonsensical predictions when used during inference.

Training output tile size $= f^l$: In this case, all output functions of the U-Net are considered during training in each batch. However, some pairs of functions that predict neighboring outputs during inference are never considered as neighbors during training. E.g. for $d = 1$, u_0 and u_{f^l-1} never predict directly neighboring embeddings during training, and hence never contribute to the same pull force loss term as direct neighbors. They do, however, predict directly neighboring embeddings during inference, no matter if stitching f^l -sized output tiles or employing larger output tiles (potentially alleviating the need for stitching) during inference. Consequently, in this case, embeddings predicted at neighboring pixels at f^l -grid-boundaries may be inconsistent.

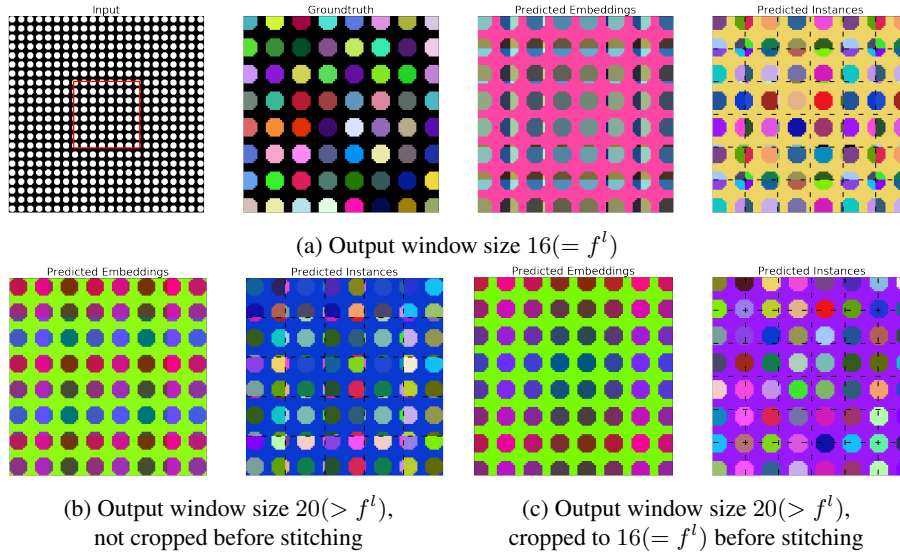


Fig. 3: Stitching issues, and how to fix them, for a U-Net with $l = 4$ and $f = 2$. (a) Training with output window edge length $w = f^l$ yields inconsistencies at f^l -grid boundaries (black dashed lines) in larger outputs. To avoid inconsistencies, not only is it necessary to (b) train with $w > f^l$, which still yields inconsistencies at stitching boundaries (black dashed lines) when naively stitching w -sized tiles, but also to (c) crop tiles to edge length $n \cdot f^l$ before stitching, with $n \geq 1$, which solves the issue.

Training output tile size $> f^l$: All possible direct neighborhoods of output functions are considered during training, given that inference output tile size is a multiple of f^l .

Inference output tile size $\neq n \cdot f^l$: Similar to the case of training output tile size $= f^l$, functions that predict neighboring outputs on two sides of a stitching boundary have never contributed to the same pull force term as neighbors during training (assuming batch size 1). Consequently, inconsistencies may occur at stitching boundaries.

Zero padding: A U-Net with zero padding, training output window size w , and sufficiently large receptive field implements up to w^d relative-distinct functions [8]. Assuming batch size 1, this yields inconsistencies at stitching boundaries analogous to the valid-padding cases discussed above. Note, while related work has attributed this effect to zero padding [7,17], to our knowledge, the only proposed mitigation strategy has been to use larger tiles during inference [7,17]. Valid padding has been investigated as a potential remedy [17], yet to no avail due to a lack of theoretical analysis.

Necessary rules to avoid inconsistencies at stitching boundaries: Following from the above considerations, in general, to avoid inconsistencies in a tile-and-stitch approach, at training time, assuming standard batch size 1 and valid convolutions, it is necessary to train with output window size strictly greater than f^l . Furthermore, at test time, it is necessary to crop output tiles of size $\neq n \cdot f^l$ to some $n \cdot f^l$ before stitching ($n \geq 1$). Figure 3 showcases the necessity of following the above rules on synthetic

images of periodically arranged disks. For the case of zero padding, training with batch size > 1 is necessary to avoid inconsistencies, where training output tiles in a batch have to be directly neighboring. For d -dimensional images, the minimum batch size that allows for considering all direct neighborhoods of U-Net functions in each batch is $d+1$. Note, however, that batch size > 1 is uncommon due to GPU memory limitations, and hence may entail further architectural changes to be feasible.

3.3 Location awareness

Corollary 4. *A U-Net with valid padding and learnt upsampling has the capacity to assign a unique ID to each pixel in an output window of size f^{dl} , independent of the specific input image.*

Proof. Proof by construction: Set the first convolution to weights zero and bias 1. This yields a constant feature map. Set all other convolutions to identity. Thus, a feature map in the bottleneck layer will be constant. Ignore skip connections by setting respective convolution kernel entries to zero. Construct upsampling filter kernels $p_1 \dots p_l$ by filling them with non-repeating prime numbers. For this, $l \cdot f^d$ prime numbers are needed. Each of the f^{dl} output functions u_i of this U-Net instance yields a product over a unique set of l distinct prime numbers. As the decomposition of any number into prime factors is unique, respective outputs effectively assign a unique ID to each output pixel. \square

Figure 4 showcases the level of location awareness that can be reached with a U-Net with valid padding and learnt upsampling. This U-Net is not constructed, but trained via metric learning with discriminative loss [6] to segment pixels as individual instances given a constant input image, thereby confirming that a U-Net instance akin to the above construction can be trained in practice. A comparable effect of location awareness has been described for zero-padding [8], which we showcase in Figure 5.

Assigning unique IDs to pixels is yet another example of reaching the upper bound of distinguishing f^{dl} instances (cf. Fig. 2), namely for the extreme case that each pixel in a constant input image forms an individual instance. However, this can only be achieved with learnt upsampling, or non-valid padding (cf. [8]). This is because for

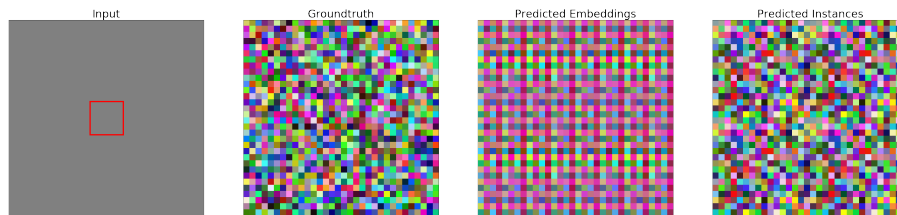


Fig. 4: A U-Net with valid padding and learnt upsampling can learn to assign a unique ID to each pixel in an output window of edge length f^l , independent of the input image. This is not possible with nearest-neighbor upsampling. Showcase: $l = 4$, $f = 2$, input image $I \equiv 1$. Output: repeating pattern of $f^{dl} = 256$ unique IDs.

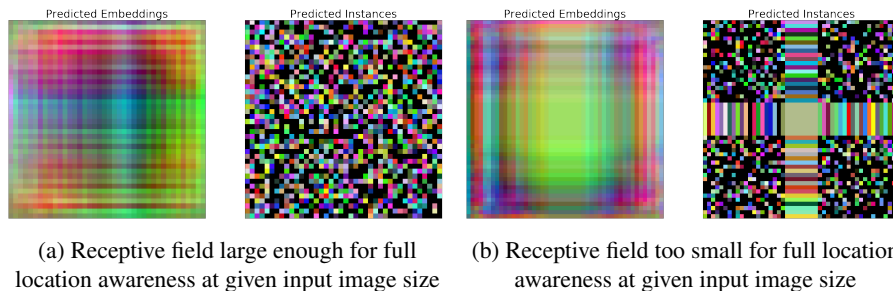


Fig. 5: A U-Net with zero-padding yields location awareness also with nearest-neighbor upsampling, if (a) each output pixel has a unique receptive field that reaches the image boundary. Otherwise, for a constant input image, (b) some pixels will necessarily receive equal outputs. Showcase: $l = 2$, $f = 2$, input image $I \equiv 1$.

valid padding and fixed upsampling, a constant input image is always mapped to a constant output image.

To our knowledge, our work is first to report that location awareness can be achieved with valid padding, thereby raising the question whether approaches that explicitly consider pixel locations or some other form of pixel IDs as additional inputs might be obsolete in case of valid padding and learnt upsampling.

3.4 Practical Impact of Noise and Small Deformations

For an infinite image of periodic- f^l arranged objects, while a U-Net with l levels and pooling factor f fails to discriminate any instances (Fig. 2a), we showcase in Fig. 6 that it may suffice to add slight Gaussian noise or small random elastic deformations to the input image to "fix" the shift equivariance problem. Here, we generate noise or deformations randomly, on-the-fly per training step as well as at test time. Hence the observed effect is not due to over-fitting to a particular noisy/deformed image.

However, note that neither noise nor elastic deformations do anything to fix the issue of inconsistencies in a tile-and-stitch approach if stitching is not performed according to the rules derived in section 3.2, as illustrated in Fig. 7.

4 Conclusion

Our work analyzes the impact of shift equivariance properties of common encoder-decoder style CNNs on the task of metric learning for instance segmentation. Contrary to a range of works that have dismissed it as fundamentally flawed due to the assumed shift equivariance of CNNs, our theoretical analysis reveals the precise shift equivariance properties of U-Net style CNNs, from which follows that a U-Net with l levels and downsampling factor f is indeed able to distinguish up to f^{dl} identical-looking (in terms of their respective receptive fields) instances in a d -dimensional image, given that object spacing is co-prime to f^l in any dimension. Furthermore, we showcase that

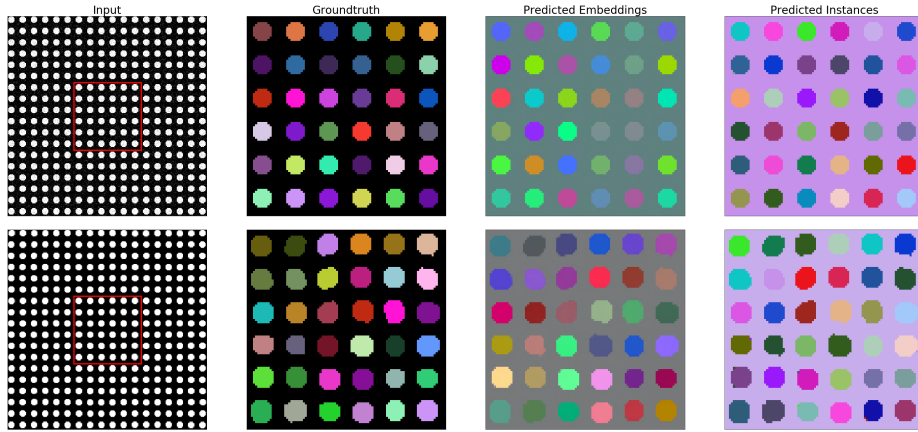


Fig. 6: Showcase of slight Gaussian noise (top row) or small random elastic deformations (bottom row) enabling a U-Net to distinguish objects that are otherwise indistinguishable due to object spacing f^l . $l = 4$, $f = 2$, learnt upsampling. Noise and deformations only visible on screen and with large zoom.

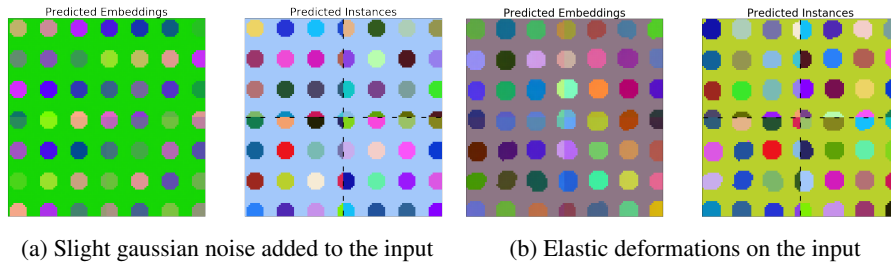


Fig. 7: Slight Gaussian noise or random elastic deformations effectively render objects at spacing f^l distinguishable (cf. Fig. 6), yet they do not affect the issue of inconsistencies in a tile-and-stitch approach if output tiles are not cropped to edge length $n \cdot f^l$ before stitching. Showcase: $l = 4$, $f = 2$, output tile edge length $w = 52 = 3 \cdot 2^4 + 4$.

adding barely visible amounts of noise or elastic deformation can enable a U-Net to distinguish objects even at "unfortunate" object spacing f^l .

We deem of even greater impact to practitioners our theoretical analysis of inconsistencies that have been reported when performing metric learning with discriminative loss for instance segmentation in a tile-and-stitch approach due to large, GPU-memory-busting inputs. To this end, our theoretical analysis of shift equivariance allows us to derive a simple set of rules that necessarily have to be followed to avoid inconsistencies at stitching boundaries when performing inference on large data. While our impact analysis in this work is tailored to metric learning with discriminative loss, the same theory of shift equivariance will yield similar implications for other pixel-wise predic-

tion tasks for which tile-and-stitch issues with inconsistencies have been reported, like semantic segmentation or image registration, to be investigated in future work.

Acknowledgments. We wish to thank Anna Kreshuk and Fred Hamprecht for inspiring discussions. J.L.R. was funded by the German Research Foundation DFG RTG 2424 *CompCancer*. M.D., P.H., L.M., A.M. and D.K. were funded by the Berlin Institute of Health and the Max Delbrueck Center for Molecular Medicine. P.H. was funded by the MDC-NYU exchange program and HFSP grant RGP0021/2018-102. X.Y. was funded by the Helmholtz Einstein International Berlin Research School in Data Science *HEIBRiDS*. V.G. was funded by the German Research Foundation DFG CRC 1404 *FONDA*. P.H., L.M. and D.K. were supported by the HHMI Janelia Visiting Scientist Program.

References

1. Alsallakh, B., Kokhlikyan, N., Miglani, V., Yuan, J., Reblitz-Richardson, O.: Mind the pad-cnns can develop blind spots. arXiv preprint arXiv:2010.02178 (2020)
2. Azulay, A., Weiss, Y.: Why do deep convolutional networks generalize so poorly to small image transformations? arXiv preprint arXiv:1805.12177 (2018)
3. Cantor, G.: Ein beitrage zur mannigfaltigkeitslehre. *Journal für die reine und angewandte Mathematik* **84**, 242–258 (1877), <http://eudml.org/doc/148353>
4. Chen, L., Strauch, M., Merhof, D.: Instance segmentation of biomedical images with an object-aware embedding learned with local constraints. In: *International Conference on Medical Image Computing and Computer-Assisted Intervention*. pp. 451–459. Springer (2019)
5. Cohen, T., Welling, M.: Group equivariant convolutional networks. In: *International Conference on Machine Learning*. pp. 2990–2999 (2016)
6. De Brabandere, B., Neven, D., Van Gool, L.: Semantic instance segmentation with a discriminative loss function. arXiv preprint arXiv:1708.02551 (2017)
7. Huang, B., Reichman, D., Collins, L.M., Bradbury, K., Malof, J.M.: Tiling and stitching segmentation output for remote sensing: Basic challenges and recommendations. arXiv preprint arXiv:1805.12219 (2018)
8. Kayhan, O.S., Gemert, J.C.v.: On translation invariance in cnns: Convolutional layers can exploit absolute spatial location. In: *Proceedings of the IEEE/CVF Conference on Computer Vision and Pattern Recognition*. pp. 14274–14285 (2020)
9. Kulikov, V., Lempitsky, V.: Instance segmentation of biological images using harmonic embeddings. In: *Proceedings of the IEEE/CVF Conference on Computer Vision and Pattern Recognition*. pp. 3843–3851 (2020)
10. Kulikov, V., Yurchenko, V., Lempitsky, V.: Instance segmentation by deep coloring. arXiv preprint arXiv:1807.10007 (2018)
11. Lee, K., Lu, R., Luther, K., Seung, H.S.: Learning dense voxel embeddings for 3d neuron reconstruction. arXiv preprint arXiv:1909.09872 (2019)
12. Lee, K., Zung, J., Li, P., Jain, V., Seung, H.S.: Superhuman accuracy on the snemi3d connectomics challenge. arXiv preprint arXiv:1706.00120 (2017)
13. Liu, R., Lehman, J., Molino, P., Petroski Such, F., Frank, E., Sergeev, A., Yosinski, J.: An intriguing failing of convolutional neural networks and the coordconv solution. *Advances in Neural Information Processing Systems* **31**, 9605–9616 (2018)

14. Neven, D., Brabandere, B.D., Proesmans, M., Gool, L.V.: Instance segmentation by jointly optimizing spatial embeddings and clustering bandwidth. In: Proceedings of the IEEE/CVF Conference on Computer Vision and Pattern Recognition. pp. 8837–8845 (2019)
15. Novotny, D., Albanie, S., Larlus, D., Vedaldi, A.: Semi-convolutional operators for instance segmentation. In: Proceedings of the European Conference on Computer Vision. pp. 86–102 (2018)
16. Odena, A., Dumoulin, V., Olah, C.: Deconvolution and checkerboard artifacts. *Distill* **1**(10), e3 (2016)
17. Reina, G.A., Panchumarthy, R., Thakur, S.P., Bastidas, A., Bakas, S.: Systematic evaluation of image tiling adverse effects on deep learning semantic segmentation. *Frontiers in Neuroscience* **14**, 65 (2020)
18. Ronneberger, O., Fischer, P., Brox, T.: U-net: Convolutional networks for biomedical image segmentation. In: International Conference on Medical Image Computing and Computer-Assisted Intervention. pp. 234–241. Springer (2015)
19. Rosenberg, A.L.: Efficient pairing functions - and why you should care. *International Journal of Foundations of Computer Science* **14**(01), 3–17 (2003)
20. Rumberger, J.L., Mais, L., Kainmueller, D.: Probabilistic deep learning for instance segmentation. arXiv preprint arXiv:2008.10678 (2020)
21. Scherer, D., Müller, A., Behnke, S.: Evaluation of pooling operations in convolutional architectures for object recognition. In: International Conference on Artificial Neural Networks. pp. 92–101. Springer (2010)
22. Stringer, C., Michaelos, M., Pachitariu, M.: Cellpose: a generalist algorithm for cellular segmentation. *bioRxiv* (2020)
23. Zhang, R.: Making convolutional networks shift-invariant again. arXiv preprint arXiv:1904.11486 (2019)

A.1 Appendix: Examples for equality of U-Net functions u

Example 1: For a U-Net with identity convolutions, weights 0 for skip connections, and fixed upsampling, functions u that merely pass the value of a bottleneck pixel through to the output (cf. Fig. 1) are absolute-equal, yet relative-distinct. Example 2: For a U-Net with output tile size $w = 1$ (i.e. a single output pixel per tile), employed in a sliding-window fashion (cf. Sec. 2.1), all functions u are relative-equal, yet absolute-distinct.

A.2 Appendix: Proof of Lemma 1, Part II

An operator F operating on images I is *shift equivariant to image shifts t* iff shifting any input image I by t causes an equal or proportional shift t' in the function's output, i.e. $\forall I \forall x : T_{t'}(F(I))(x) = F(T_t(I))(x)$. In case $t = t'$, we call F shift equivariant to input shifts t . In case $t \neq t'$, we call F shift equivariant to input shifts t at output shifts t' . In the following, we prove that any U-Net with l pooling layers and pooling factor f is shift equivariant to image shifts $f^l t$, $t \in \mathbf{Z}$. Without loss of generality, we consider one-dimensional, one-channel input images, and one-channel feature maps throughout. A U-Net is composed of an encoder path and a decoder path:

Encoder Path. An encoder block is composed of a number of conv+ReLU layers. We refer to the function implemented by the i -th encoder block as E_i . The output of E_i is passed through a max pooling layer, referred to as MP_i . We refer to the composition of E_i and MP_i as EMP_i . The convolution operator F_{conv} (stride=1) is commonly defined as $F_{conv}(g)(x) = (g \star h)(x) = \sum_{m \in \mathbf{Z}} g(m)h(m-x)$ (see e.g. [5]), and well-known and easily shown to be shift equivariant to any shifts t :

$$\begin{aligned} F_{conv}(T_t(g))(x) &= \sum_{m \in \mathbf{Z}} g(m-t)h(m-x) = \sum_{m' \in \mathbf{Z}} g(m')h(m'+t-x) \\ &= \sum_{m' \in \mathbf{Z}} g(m')h(m'-(x-t)) = T_t(F_{conv}(g))(x) \end{aligned} \quad (4)$$

The same holds for the ReLU operator: $ReLU(T_t(g))(x) = \max(0, T_t(g)(x)) = \max(0, g(x-t)) = T_t(ReLU(g))(x)$. Compositions of shift equivariant operators are also shift equivariant, hence E_i is shift equivariant to any input shifts t . To analyze MP_i , we break it down into the max pooling operator $\psi_f(g)(x) := \max\{g(x+i) \mid i \in \{0, \dots, f-1\}\}$ with kernel size f , and the sub-sampling operator $s_f(g)(x) := g(fx)$ at stride f . Analogous to ReLU, ψ_f is shift equivariant to any shift t ,

$$\begin{aligned} \psi_f(T_t(g))(x) &= \max\{T_t(g)(x+i) \mid i \in \{0, \dots, f-1\}\} \\ &= \max\{g(x+i-t) \mid i \in \{0, \dots, f-1\}\} = T_t(\psi_f(g))(x), \end{aligned} \quad (5)$$

while $T_t(s_f(g))(x) = s_f(T_{ft}(g))(x)$, i.e. s_f is shift equivariant to input shifts ft at proportional shifts t of the output. With this we get

$$\begin{aligned} EMP_i(T_{ft}(g))(x) &= s_f(\psi_f(E_i(T_{ft}(g))))(x) = s_f(T_{ft}(\psi_f(E_i(g))))(x) \\ &= T_t(s_f(\psi_f(E_i(g))))(x) = T_t(EMP_i(g))(x), \end{aligned} \quad (6)$$

i.e., an encoder block with max pooling with downsampling factor f is shift equivariant to input shifts ft at proportional output shifts t . Overall, a general encoder path E

employs l downsampling operations with factors f_1, \dots, f_l . Shift equivariance proportionality factors multiply when composing operators, hence the encoder path is shift equivariant to input shifts $t \prod_1^l f_i$ at output shifts t . In the family of U-Nets we consider, $f_i = f_j$ for all i, j , yielding shift equivariance to input shifts tf^l at output shifts t : $E(T_{tf^l}(I))(x) = T_t(E(I))(x)$.

Decoder Path. The decoder path is composed of decoder blocks D_i , whose output is passed through respective upsampling layers, referred to as UP_i . A decoder block has the same form as an encoder block, i.e. it consists of a number of conv+ReLU layers, and is thus shift equivariant. We refer to the composition of D_i and UP_i as DUP_i . Upsampling is either *learnt*, i.e. performed via up-convolution with trainable kernel function $p(x)$, with kernel size = stride = f (also called upsampling factor), or performed via nearest neighbor interpolation. We treat both in one go, as the latter is a special case of the former with fixed kernel function $p(x) \equiv 1$. We can express the up-convolution operator UP_i with upsampling factor f as $UP_i(g)(x) = (g * p)(x) = \sum_{m \in \mathbf{Z}} g(m)p(x - fm)$. Concerning its shift equivariance,

$$\begin{aligned} UP_i(T_t(g))(x) &= \sum_{m \in \mathbf{Z}} g(m-t)p(x-fm) = \sum_{m' \in \mathbf{Z}} g(m')p(x-f(m'+t)) \\ &= \sum_{m' \in \mathbf{Z}} g(m')p((x-ft)-dm') = T_{ft}(UP_i(g))(x), \end{aligned} \quad (7)$$

i.e., upsampling with factor f is shift equivariant to input shifts t at output shifts ft . Thus a decoder block with subsequent upsampling layer, DUP_i , is also shift equivariant to input shifts t at output shifts ft : $DUP_i(T_t(g))(x) = T_{ft}(DUP_i(g))(x)$. Concerning the input to DUP_i , at the bottleneck level $i = l$, this is the output of EMP_l . Concerning shift equivariance of their composition $U_l := DUP_l \circ EMP_l$, assuming equal down- and upsampling factors f , we get

$$\begin{aligned} U_l(T_{ft}(g))(x) &= DUP_l(EMP_l(T_{ft}(g)))(x) = DUP_l(T_t(EMP_l(g)))(x) \\ &= T_{ft}(DUP_l(EMP_l(g)))(x) = T_{ft}(U_l(g))(x), \end{aligned} \quad (8)$$

i.e., U_l is shift invariant to shifts ft . For $i < l$, the input to DUP_i is a multi-channel image formed by concatenating the output of DUP_{i+1} and the output of encoder block E_{i+1} . Referring to the composition of all U-Net blocks up to a block B as \tilde{B} , we can write the input to DUP_i as $(T_{\Delta x_{i+1}}(\tilde{E}_{i+1}(I)), \tilde{DUP}_{i+1}(I))$. Here, Δx_{i+1} is the shift required to centrally align $\tilde{E}_{i+1}(I)$ and $\tilde{DUP}_{i+1}(I)$, as $\tilde{DUP}_{i+1}(I)$ is of size smaller or equal than $\tilde{E}_{i+1}(I)$. All Δx_i are fixed for a given architecture, and hence image concatenation is shift equivariant: $(T_{\Delta x_i}(T_t(g)), T_t(q))(x) = T_t((T_{\Delta x_i}(g), q))(x)$. Consequently, just like DUP_l , for $i < l$, DUP_i is shift equivariant to input shifts t at output shifts ft . Furthermore, as proportional shift equivariance factors multiply when composing respective operators, analogous to $U_l := DUP_l \circ EMP_l$, we get that the composition of all blocks from EMP_i to DUP_i , $U_i := DUP_i \circ U_{i+1} \circ EMP_i$, is shift equivariant to shifts $f^{l-i+1}t$. In particular, U_1 is shift equivariant to shifts $f^l t$.

To yield the full U-Net function U , the outputs of U_1 and E_1 are concatenated into a multi-channel image, which is passed through a final shift invariant decoder block D_0 , $U := D_0((T_{\Delta x_1} E_1(I), U_1(I)))$. Thus U is equally shift equivariant as U_1 , i.e., the U-Net is shift equivariant to shifts $f^l t$. \square